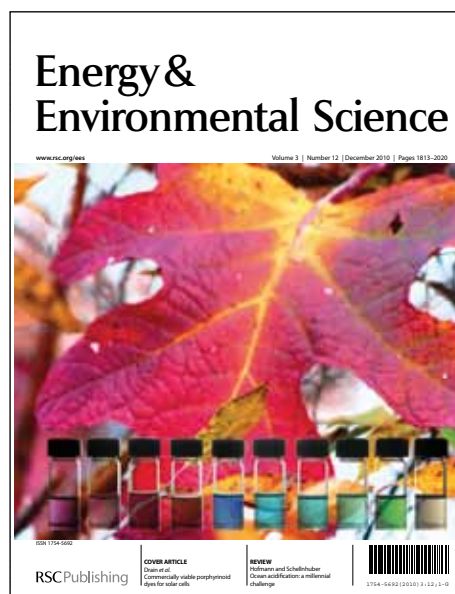


# Energy & Environmental Science

## Accepted Manuscript



This is an *Accepted Manuscript*, which has been through the RSC Publishing peer review process and has been accepted for publication.

*Accepted Manuscripts* are published online shortly after acceptance, which is prior to technical editing, formatting and proof reading. This free service from RSC Publishing allows authors to make their results available to the community, in citable form, before publication of the edited article. This *Accepted Manuscript* will be replaced by the edited and formatted *Advance Article* as soon as this is available.

To cite this manuscript please use its permanent Digital Object Identifier (DOI®), which is identical for all formats of publication.

More information about *Accepted Manuscripts* can be found in the [Information for Authors](#).

Please note that technical editing may introduce minor changes to the text and/or graphics contained in the manuscript submitted by the author(s) which may alter content, and that the standard [Terms & Conditions](#) and the [ethical guidelines](#) that apply to the journal are still applicable. In no event shall the RSC be held responsible for any errors or omissions in these *Accepted Manuscript* manuscripts or any consequences arising from the use of any information contained in them.

# Soft X-ray XANES Studies of Various Phases Relating to $\text{LiFePO}_4$ Based Cathode Materials

Songlan Yang,<sup>\*1,2</sup> Dongniu Wang,<sup>1,2</sup> Guoxian Liang,<sup>3</sup> Yun Miu Yiu,<sup>2</sup> Jiajun Wang,<sup>1</sup> Lijia Liu<sup>2</sup>, Xueliang Sun,<sup>\*1</sup> and Tsun-Kong. Sham<sup>\*2</sup>

<sup>1</sup>*Department of Mechanical and Materials Engineering, University of Western Ontario, London, Ontario, N6A 5B9 Canada*

<sup>2</sup>*Department of Chemistry, University of Western Ontario, London, Ontario, N6A 5B7 Canada*

<sup>3</sup>*Phostec Lithium Inc, 1475 Rue Marie-Victorin, St-Bruno, QC, J3V 6B7 Canada*

$\text{LiFePO}_4$  has been a promising cathode material for rechargeable lithium ion batteries. Different secondary or impurity phases, forming during either synthesis or subsequent redox process under normal operating conditions, can have a significant impact on the performance of the electrode. The exploration of the electronic and chemical structures of impurity phases is crucial to understand such influence. We have embarked on a series of synchrotron-based x-ray absorption near-edge structure (XANES) spectroscopy studies for the element speciation in various impurity phase materials relevant to  $\text{LiFePO}_4$  for Li ion battery. In the present report, soft-X-ray XANES spectra of Li *K*-edge, P *L*<sub>2,3</sub>-edge, O *K*-edge and Fe *L*<sub>2,3</sub>-edge have been obtained for  $\text{LiFePO}_4$  in crystalline, disordered and amorphous forms and some possible “impurities”, including,  $\text{LiPO}_3$ ,  $\text{Li}_4\text{P}_2\text{O}_7$ ,  $\text{Li}_3\text{PO}_4$ ,  $\text{Fe}_3(\text{PO}_4)_2$ ,  $\text{FePO}_4$ , and  $\text{Fe}_2\text{O}_3$ . The results indicate that each element from different pure reference compounds exhibit unique spectral features in terms of energy position, shape and intensity of the resonances in their XANES. In addition, Inverse partial fluorescence yield (IPFY) reveals the surface vs. bulk property of the specimens. Therefore, the spectra data provided here can be used as standards in the future for phase composition analysis.

---

\*Email: [songlan.yang@lightsource.ca](mailto:songlan.yang@lightsource.ca); [xsun@eng.uwo.ca](mailto:xsun@eng.uwo.ca), [tsham@uwo.ca](mailto:tsham@uwo.ca).

## Introduction

The boom in portable telecommunications, computer equipment as well as electric and hybrid vehicles has created a growing demand for safe and advanced lithium-ion batteries with high energy density, good reversibility, low cost, long lifetime, small size and light weight. Currently, the most popular commercial cathode materials for lithium-ion batteries are based on transition metal oxide  $\text{LiCoO}_2$ .<sup>1</sup> Unfortunately,  $\text{LiCoO}_2$  based cathode materials suffer from some disadvantages and hence are limited to small scale lithium-ion battery applications. For example,  $\text{LiCoO}_2$  is costly and toxic. And its layered structure undergoes large volume change during oxidation-reduction (redox) process, which limits the attainment of full reversibility.<sup>2</sup> It is metastable when fully charged, and on overcharging at temperatures above 200 °C. Also they release oxygen from the cathodes increasing the possibility of organic electrolytes decomposition, which generates undesired heat.

Intensive research has been focused on developing alternative cathode materials for cost, safety, environment and service life concerns.  $\text{LiFePO}_4$  is one of the promising candidate materials in this regard. The reversible lithium insertion-extraction for  $\text{LiFePO}_4$  was firstly reported by Goodenough et al. in 1997.<sup>3</sup> This material is environmentally benign, inexpensive and thermally stable. Furthermore, it has a relatively high theoretical specific capacity of 170  $\text{mAh}\cdot\text{g}^{-1}$ , a good cycling stability, and a flat discharge potential of 3.4 V versus  $\text{Li}/\text{Li}^+$ .  $\text{LiFePO}_4$  has an olivine structure (space group: Pnma), in which Li, Fe, and P atoms occupy octahedral 4a, octahedral 4c, and tetrahedral 4c site, respectively. Like any lithium battery materials, during charge,  $\text{Li}^+$  ions are removed from the  $\text{LiFePO}_4$  cathode and stored in the anode, often made of carbon. During discharge, the  $\text{Li}^+$  ions leave the anode and return to the  $\text{LiFePO}_4$  crystal, and the electrons flow through an external circuit. It is called delithiation when the  $\text{Li}^+$  ions are removed from  $\text{LiFePO}_4$ . When the  $\text{Li}^+$  ions are reintroduced to  $\text{FePO}_4$  to form  $\text{LiFePO}_4$ , it is called lithiation. The main problem associated with this material is its poor rate capability, due to its low electric conductivity and slow lithium ion diffusion kinetics<sup>4,5</sup> Fortunately, these problems can be partly overcome by optimizing the synthesis route of  $\text{LiFePO}_4$  through coating the material with high conductivity materials like carbon,<sup>6-8</sup> and decreasing the grain size of the material to nano-scale to shorten the diffusion path length of the electrons and  $\text{Li}^+$  ions.<sup>9</sup>

To guide the synthesis of  $\text{LiFePO}_4$  based cathode materials, Ceder and co-workers developed the Li-Fe-P-O<sub>2</sub> phase diagram as a function of oxidation conditions from first principle calculations,<sup>10, 11</sup> which agrees with the experimental results. The key factor to optimize synthesis route is the thorough understanding of phase equilibria under both stoichiometric and non-stoichiometric conditions.<sup>10</sup> To avoid the formation of  $\text{Fe}^{3+}$  in the material, practically,  $\text{LiFePO}_4$  is synthesized under reducing conditions. Depending on the synthesis parameters, such as precursors used, the synthesis temperature, the synthesis atmosphere (Ar or  $\text{N}_2/\text{H}_2$ ), and the degree and nature of non-stoichiometry, different impurities or secondary phases can form in addition to  $\text{LiFePO}_4$ , during either the synthesis or the following in-service process.<sup>10</sup> For example, with the excess of lithium in the system, some lithium phosphates, like  $\text{Li}_3\text{PO}_4$ ,  $\text{Li}_4\text{P}_2\text{O}_7$  and  $\text{LiPO}_3$ , may co-exist with  $\text{LiFePO}_4$ .<sup>10, 11</sup>

The nature of these impurities or secondary phases in the cathode can have significant influence on the performance of the batteries. In case of the presence of undesirable or insulating phases, they may degrade the structure and electrochemical reactivity of the material hence the capacity of the electrode and have an adverse effect on the electrochemical performance. On the other hand, some electronic or ionic conductive secondary phases may improve the performance of the electrode, for example, by acting as electron donors to enhance the electrical conductivity of  $\text{LiFePO}_4$  to enable the high charging and discharging rate of the battery. It was reported that,  $\text{Fe}_2\text{P}$  was formed during the synthesis of phase pure  $\text{LiFePO}_4$ , which may impede the performance of the material.<sup>12</sup> Latter, Subramanya Herle *et al.*<sup>13</sup> and Xu *et al.*<sup>14</sup> reported the beneficial effect of  $\text{Fe}_2\text{P}$  on the electrochemical performance of  $\text{LiFePO}_4$ . More recently, Song and co-workers<sup>15</sup> found the amphoteric effect of  $\text{Fe}_2\text{P}$  on the performance of  $\text{LiFePO}_4$ ; i.e. that when its content was below the critical amount,  $\text{LiFePO}_4$  cathode displayed an enhanced electrochemical performance. However, when its content was above the critical content, the electrochemical performance of the  $\text{LiFePO}_4$  cathode worsened. Later, they reported that the degradation of  $\text{LiFePO}_4$  cathode when the amount of  $\text{Fe}_2\text{P}$  above a critical level was due to the formation of the insulating phase  $\text{Li}_4\text{P}_2\text{O}_7$ , even though, Ceder *et al.*<sup>11</sup> showed the exciting results on the positive effect of  $\text{Li}_4\text{P}_2\text{O}_7$  related surface coating on the ion-conductivity of  $\text{LiFePO}_4$ , where ultrafast charging and discharging rate had been achieved and a rate capability equivalent to full battery discharge in 10-20s was reached. The mechanism for this improvement in rate performance has not yet been understood and it is still vigorously debated in the literature<sup>16</sup>.

Therefore, much more work is desired to be conducted to clarify the impact of the impurities/secondary phases, and their assembly on the performance of  $\text{LiFePO}_4$ -based cathode materials. For this purpose, accurate characterization is crucial for the possible impurities/secondary phases which may appear during the synthesis and the service of  $\text{LiFePO}_4$  based materials.

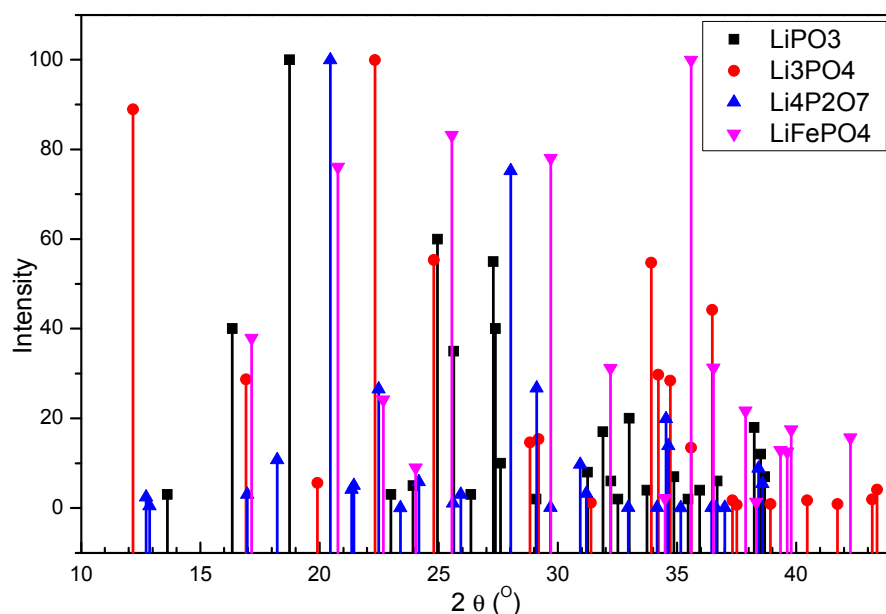


Fig. 1 Indexed XRD data for  $\text{LiFePO}_4$  (JCPDS No. 83-2092),  $\text{LiPO}_3$  (JCPDS No. 26-1177),  $\text{Li}_3\text{PO}_4$  (JCPDS No. 84-0046) and  $\text{Li}_4\text{P}_2\text{O}_7$  (JCPDS No. 77-1045)

The structure and phase purity of  $\text{LiFePO}_4$  are mostly and often characterized by X-ray diffraction (XRD). Fig.1 shows the comparison of theoretical XRD patterns between some lithium phosphate, including  $\text{LiPO}_3$ ,  $\text{Li}_3\text{PO}_4$ , as well as  $\text{Li}_4\text{P}_2\text{O}_7$ , and  $\text{LiFePO}_4$ . It is apparent from Fig.1 that the  $2\theta$ s (positions) of the peaks for these different compounds are very close, and in some cases, peaks overlap with each other. Therefore, it is difficult to discern these phases, especially when the content of such impurity phases is low. As mentioned earlier, nano-structured materials have received much attention recently as potential electrode materials for lithium ion batteries. As the grain size becomes nanometer scale, the widening of the peaks in XRD patterns will introduce further challenges in phase identification. Ceder *et al.* used X-ray photoelectron spectroscopy (XPS) to distinguish between  $\text{Li}_4\text{P}_2\text{O}_7$  from  $\text{LiFePO}_4$  by the phosphorus 2p binding energy. But the difference in the phosphorus 2p binding energy of these two compounds is very small, as a result, the profiles for phosphorus 2p XPS spectra from

LiFePO<sub>4</sub> and LiFePO<sub>4</sub>-Li<sub>4</sub>P<sub>2</sub>O<sub>7</sub> composites are very similar.<sup>11</sup> Further, the analysis of lithium 1s binding energy through XPS becomes more difficult due to its overlap with the 3p binding energy of iron. Besides, when the Mg K $\alpha$  line is used as the excitation source in XPS measurement, the photoionization cross-section of the iron 3p electron is higher than that of the lithium 1s electron hampering its sensitivity in Li detection.<sup>17</sup> Further still, no systemic study on the application of XPS in the characterization of various lithium phosphates, including LiPO<sub>3</sub>, Li<sub>3</sub>PO<sub>4</sub>, and Li<sub>4</sub>P<sub>2</sub>O<sub>7</sub> has been reported in the literature.

The synchrotron-based X-ray absorption near-edge structure (XANES) spectroscopy (sometimes also referred to as near-edge X-ray absorption fine structure (NEXAFS) spectroscopy) is a molecular-scale spectroscopy technique that yields electronic and structural information on the element of interest by deriving information from the modulation of the absorption coefficient above a particular edge of an element using the tuneable, very bright and polarized synchrotron light.<sup>18</sup> XANES is element and core level specific and is sensitive to the local bonding environment and it offers a possibility to overcome the specific limitations of the above-discussed methods for the characterization of the phase compositions of LiFePO<sub>4</sub>-based cathode materials with different impurities. Each XANES spectrum, displays the absorption coefficient from 10 to 20 eV below to ~ 30 to 50 eV above an absorption edge of a core level of an element (e.g. 1s of Li, L<sub>3,2</sub> of Fe) as a function of excitation energy is usually characterized by intense resonance features, arising from excitations of core-level electrons to unoccupied orbitals that are bound, quasi-bound and continuum levels and from multiple scattering of the emitted photoelectrons by the geometrical arrangement of neighbouring atoms around the absorbing atom.<sup>19</sup>

Although, the application of synchrotron XANES techniques on the study of structure changes of LiFePO<sub>4</sub> cathode materials during the charge/discharge cycling process have been reported by several researchers,<sup>20-31</sup> the information is only limited to the LiFePO<sub>4</sub>/FePO<sub>4</sub> two-phase system (with the fully charge state, the cathode materials is LiFePO<sub>4</sub>, while, with the fully discharge state, the cathode is composed of FePO<sub>4</sub>, and in-between the cathode is composed of two phases, LiFePO<sub>4</sub> and FePO<sub>4</sub>) on the Fe *K*-edge,<sup>20-26, 28</sup> Fe *L*-edge,<sup>21, 22, 27</sup> O *K*-edge,<sup>21, 22</sup> and P *K*-edge.<sup>29</sup> No report regarding the XANES spectra of Li *K*-edge in this system can be found to the best of our knowledge. Therefore, exploration of the roles of other impurities or secondary phases like LiPO<sub>3</sub>, Li<sub>3</sub>PO<sub>4</sub>, and Li<sub>4</sub>P<sub>2</sub>O<sub>7</sub> on the battery performance is much desirable.

We have recently embarked on a program on the X-ray absorption spectroscopy studies of  $\text{LiFePO}_4$  and related materials. We will use synchrotron-based soft X-ray XANES to characterize the electronic and chemical structures of all possible compounds existing in the  $\text{LiFePO}_4$ -based cathode materials for lithium ion batteries by XANES of the Li  $K$ -, O  $K$ -, P  $L_{2,3}$ - and Fe  $L_{2,3}$ -edges under consistent experimental conditions and possibly Fe and P  $K$ -edge. The first results reported here indicate that each element from different pure reference compounds shows specific spectral features, and hence these data can be used as standards for future  $\text{LiFePO}_4$ -based phase composition analysis. This information is very useful to the understanding of the performance of the batteries and the development of better cathode materials. We report here the XANES systematic of a series of  $\text{LiFePO}_4$  and related compounds of interest.

## Experimental

Ten reference compounds, including  $\text{Li}_2\text{CO}_3$ ,  $\text{Li}_4\text{P}_2\text{O}_7$ ,  $\text{Li}_3\text{PO}_4$ ,  $\text{LiPO}_3$ ,  $\text{LiFePO}_4$ ,  $\text{Fe}_3(\text{PO}_4)_2$ ,  $\text{FePO}_4 \cdot 2\text{H}_2\text{O}$  and  $\text{Fe}_2\text{O}_3$  have been used for the present study. Of the  $\text{LiFePO}_4$  (LFP) samples, three different polymorphs, crystalline, disordered and amorphous, hence forth denoted c-LFP, d-LFP and a-LFP are also studied. The XRD of these samples are shown in Figure 2. From Figure 2, judging from the relative intensity and the sharpness of the diffraction peaks, their corresponding labeling is immediately apparent; i.e. that the sample with the most intense and well defined sharp diffraction pattern is labeled c-LFP, the sample with somewhat broadened diffraction pattern, the d-LFP and the one with no diffraction pattern a-LFP.

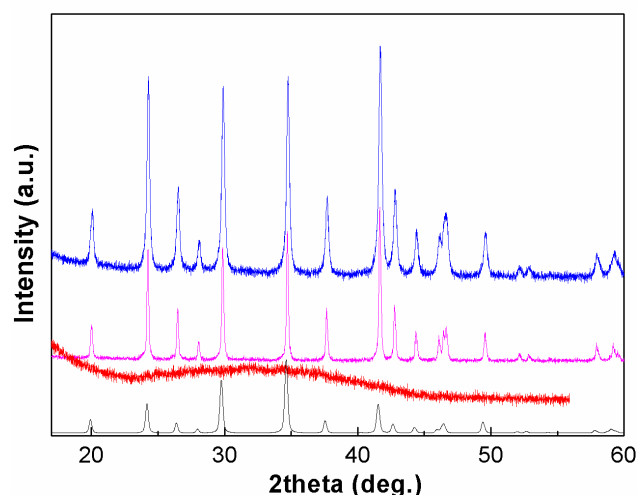


Fig. 2 XRD  $2\theta$  scan of the three  $\text{LiFePO}_4$  samples; from top to bottom: crystalline, disordered, amorphous and indexed XRD values of  $\text{LiFePO}_4$ .

All the samples are very fine powders from Phostech Lithium Inc. The powder samples were spread as very thin films onto double-sized carbon tapes attached to the sample holder, which was then inserted into the X-ray absorption vacuum chamber with base pressure of  $2 \times 10^{-8}$  torr. A very thin sample is always desirable to minimize thickness effect (self-absorption) in x-ray fluorescence yield measurements (see below). The air sensitive samples, were kept under inert atmosphere prior to its introduction into the chamber. The XANES measurements were performed at the Canadian Light Source (CLS) on the Variable Line Spacing Plane Grating Monochromator (VLS PGM) beamline for the Li K-edge and P  $L_{2,3}$ -edge spectra, and the high resolution Spherical Grating Monochromator (SGM) beamline for the O K-edge and Fe  $L_{2,3}$ -edge spectra. The CLS is a 2.9 GeV, third generation synchrotron light source, a Canadian national facility located in Saskatoon, Saskatchewan. The VLS PGM beamline uses a 185 mm planar undulator and three gratings to cover a photon energy ranged from 5.2 to 250 eV. It is capable to provide  $10^{12}$  photons per second at 100 mA at the Li K-edge and P  $L_{2,3}$ -edge with a resolution higher than 10,000 ( $E/\Delta E$ ) with an entrance and exit slit settings of 50  $\mu\text{m}$ .<sup>32</sup> In this research, the medium energy grating, which covers the energy range was used for Li K-edge measurement recorded between 50 and 100 eV. The high energy grating, which covers the energy range from 90 eV to 250 eV was used for the P  $L_{2,3}$ -edge measurement recorded from 125 to 165 eV. These gratings have been carefully tested to ensure that they do not present higher order problems. The entrance and exist slits were set at  $50 \times 50 \mu\text{m}$ . The SGM beamline uses a 45 mm planar undulator and three gratings to cover a photon energy region from 250 to 2000 eV. It offers resolution greater than 5,000  $E/\Delta E$  at energy below 1500 eV.<sup>33</sup> The beamline is capable of providing  $10^{12}$  photons per second at 250eV and exceeds  $10^{11}$  photons per second up to 1900eV at 100 mA ring current. The medium energy grating, which covers 450 to 1250 eV was used for both O K-edge and Fe  $L_{2,3}$ -edge measurement. For the O K-edge, the measurement was recorded from 515 eV to 580 eV, and for the Fe  $L_{2,3}$ -edge, the measurement was recorded from 695 eV to 740 eV. The step size was taken as 0.1 eV. In both beamlines, the angle between the incident beam and the sample surface was at normal incidence. Spectra were recorded in the fluorescence yield mode (FLY) using a microchannel-plate detector and the total electron yield (TEY) mode by measuring the sample current with a current amplifier.

The power of soft X-ray spectroscopy is its ability to discern surface and bulk signal using total electron yield and soft X-ray fluorescence yield, respectively, i.e. when surface and bulk have different composition. This comes about as the result of the relatively short inelastic free mean path (e.g. universal curve of electron escaped depth) of electrons of relatively low kinetic energy; it is the same reason why XPS is generally surface sensitive. The soft X-ray fluorescence yield on the other hand has a much longer attenuation length in solid, typically 2 orders of magnitude longer in the soft X-region if we compare the probing depth of Auger electrons versus corresponding fluorescence soft X-rays. The only drawback of X-ray fluorescence yield is the effect of saturation which tends to broaden the resonance and distort the spectrum. This deficiency is corrected by the use of Inversed partial fluorescence yield discussed below.

It should be noted that FLY measurement often suffers from self absorption, resulting in the distortion of the spectral features. This situation can be severe in soft X-ray measurements, hampering its application. However, this situation has been amended by employing the Inverse Partial Fluorescence Yield (IPFY) technique recently developed by Achkar et al.<sup>34</sup> The technique is based on a total absorption situation in which all the incident photons are absorbed and two different elements are competing for the same photon flux. Thus the fraction of photons absorbed below and above an absorption edge of one particular element changes abruptly at the expense of the other element but the incident photons are still absorbed 100%. In this particular case of LFPO, both the Fe L<sub>3,2</sub>-edge and the O K-edge are competing for photons, thus at the Fe L-edge, the fraction of incident photons absorbed by Fe increases dramatically at the expense of the O K-edge absorption, leading to a corresponding dramatic decrease in the fraction of photons absorbed by O. This behaviour is illustrated in Figure 3 where we show the 2D display of excitation energy versus X-ray fluorescence energy with the relative intensity color coded as shown on the map.

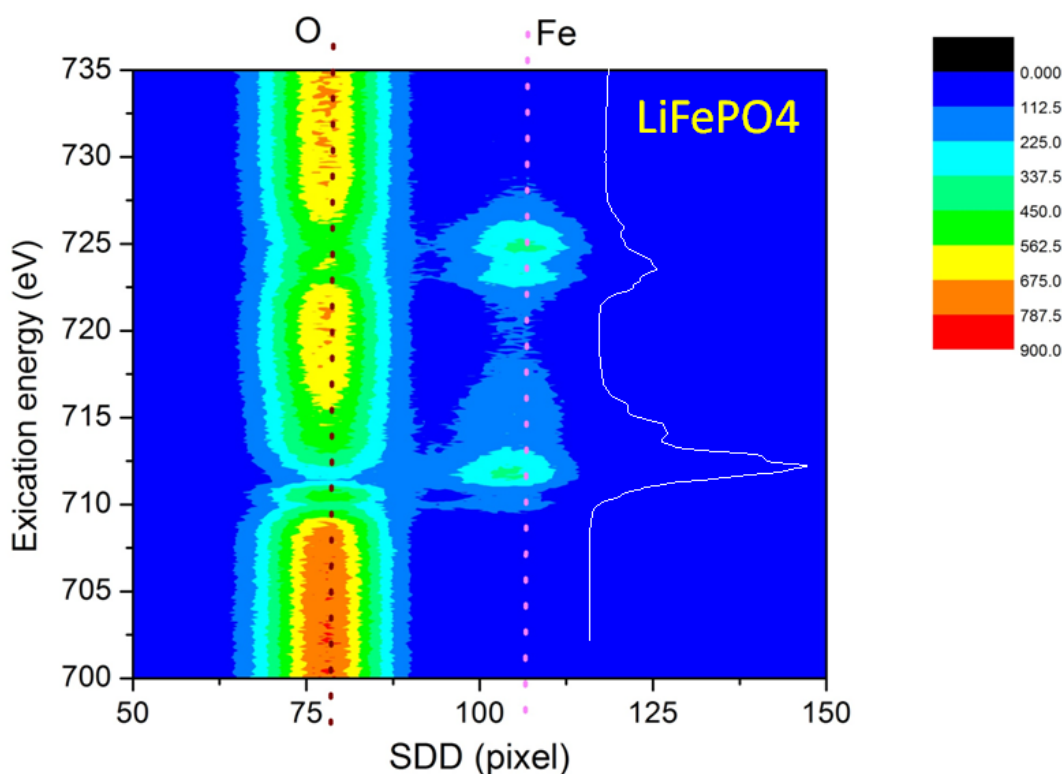


Fig. 3 2-D display of excitation energy across the Fe L<sub>3,2</sub>-edge (y-axis) vs. fluorescence/scattered X-ray energy (x-axis) from O and Fe detected with a silicon drift detector (SDD). The fluorescence X-ray energy from O K shell and Fe L<sub>3,2</sub> shell, respectively, are marked with a vertical dotted line with the intensity colour coded. The Fe L<sub>3,2</sub>-edge XANES is also shown (white trace).

By monitoring the inverse of the O fluorescence yield ( $I_o/O$  emission), we can obtain nearly self-absorption-free fluorescence yield spectra of the Fe<sub>3,2</sub> L-edge. More details have been worked out by Achkar et al<sup>34</sup>. This situation is analogous to previously studied XEOL and photoconductivity techniques.<sup>35, 36</sup> All spectra reported were normalized to the intensity of the incident beam ( $I_0$ ), measured simultaneously as the current emitted from a refreshed gold mesh located after the last optical elements of the beamline.

For a consistent data treatment, the background correction was carried out by subtracting an extrapolated linear curve between the first data point and the starting point of the first pre-edge feature using OriginPro8.1 (OriginLab, MA, USA). The non-linear background is caused by other excitations (e.g. valence electrons), low-energy electrons and sample charging when the sample is a thick non-conductor. They vary somewhat depending on the elements present in the system but remain generally monotonic. A polynomial fit was subtracted to straighten the pre-edge region in front of the first feature. All spectra are presented without additional smoothing.

## Results and discussion

### XANES spectroscopy of shallow core levels

XANES concerns with the measurement and interpretation of the X-ray absorption coefficient above an absorption edge of an element in a chemical environment. Thus it is element specific since all core levels of elements have their unique threshold energy. As the photon energy is tuned towards the absorption edge, the absorption coefficient will increase sharply (often referred to as an edge jump) when the incoming photon energy is sufficient to excite the core electron into previously unoccupied electronic states (e.g. LUMO and LOMO +1, etc. in molecules, conduction band in semiconductors and ionic materials with a large band gap, as well as the unoccupied densities of states just above the Fermi level in metals). The selection rule is dipole to a good approximation, thus Fe  $M_{3,2}$  (3p) and  $L_{3,2}$ -edge (2p) will probe the unoccupied states of Fe 3d and 4s character, the Li and O K-edge (1s) will probe the unoccupied states of p character of Li and O respectively and the P  $L_{3,2}$  edge will probe states of s and d character of P. Since the unoccupied electronic states are determined by the molecular potential due to the nearest neighboring atoms and the symmetry of the environment of the absorbing atom, XANES probe the local structure and bonding of the absorbing atom in a chemical environment.

As the photon energy increases above the threshold, the excitation will probe the unoccupied electronic states of the following nature: bound, quasi-bound and continuum. In the XANES region, we deal with transitions to the bound and quasi bound states. The bound states are below the vacuum level, thus transition to bound states tends to have longer lifetime, hence sharper peaks and more chemically sensitive. The quasi-bound states are best understood as potential

barrier states or, virtual molecular orbitals or multiple scattering states. They are states above the vacuum level arising from a barrier set up by the molecular potential unique to the chemical environment; it can be thought of as a caging effect by the surrounding atoms. Thus transition to quasi bound states tends to be short-lived, hence considerably broader than bound state transitions, since the excited electrons will ultimately tunnel out of the potential barrier. Free atom does not exhibit any modulation in XANES other than atomic Rydberg transitions (bound states) since there are no surrounding atoms and no chemical bonding although high angular momentum state can create such a barrier in high Z atoms such as the rare-earth. This situation is not relevant to our study here. Hence electron excited to a quasi-bound state has non-zero kinetic energy, but to escape into the vacuum, it needs to tunnel out the potential barrier. Another way of looking at it is that an excited electron with low kinetic energy will be in-elastically scattered by the surrounding atoms multiple times before it escapes into vacuum. This is the reason free atom exhibits monotonic coefficient without modulation above the threshold. Molecular systems exhibit relatively sharp bound to bound transitions (long lifetime) and bound to quasi bound states are broad (short lifetime) and are usually above the ionization threshold (vacuum level in molecules). The most common bound to bound and bound to quasi-bound transitions are observed as  $1s$  to  $\pi^*$  and  $1s$  to  $\sigma^*$  transitions in unsaturated molecule of low z atoms, such as CO, or in condensed matters such as graphite.<sup>35,37</sup>

### Li K-edge XANES

Fig. 4 shows the Li *K*-edge XANES spectra for lithium-containing compounds, including  $\text{LiCO}_3$ ,  $\text{Li}_3\text{PO}_4$ ,  $\text{LiPO}_3$ ,  $\text{Li}_4\text{P}_2\text{O}_7$ , amorphous  $\text{LiFePO}_4$  (a-LFP), disordered  $\text{LiFePO}_4$  (d-LFP) and crystallite  $\text{LiFePO}_4$  (c-LFP). The vertical dashed lines mark the features of interest. Compared with those reported by Tsuji *et al.*<sup>17</sup> on the Li *K*-edge XANES spectra for lithium compounds, the present results show a much improved signal to noise ratio and energy resolution, due to the very high energy resolution of the beamline as well as the high flux. The energy positions for peaks as appeared in the spectra are summarized in Table 1. The Li *K*-edge XANES spectra exhibited several features, which is unique for each individual compounds and vary among compounds. The spectroscopic details of these model compounds will be described elsewhere together with theoretical calculation.<sup>38</sup> Here, we have taken a more phenomenological approach to show the scope of the information one can obtain from a semi-quantitative analysis.

	(A)	(B)	(C)	(D)	(A')	(B')	(C')	(D')
Li <sub>2</sub> CO <sub>3</sub>	59.9	61.8		67.2				59.0
Li <sub>3</sub> PO <sub>4</sub>	59.9	61.8	64.9	67.8				
Li <sub>4</sub> P <sub>2</sub> O <sub>7</sub>	60.0		65.0	68.0				
LiPO <sub>3</sub>	60.2		65.2	68.0				
c-LFP	60.2	61.7	64.9		52.2	55.0	57.4	
d-LFP	60.2	61.7	64.9		52.2	55.0	57.4	
a-LFP	60.2		64.9		52.2	55.0	57.4	

Table 1 Energy position of Li K-edge XANES spectra of the Li containing compound in the LiFePO<sub>4</sub> based cathode materials

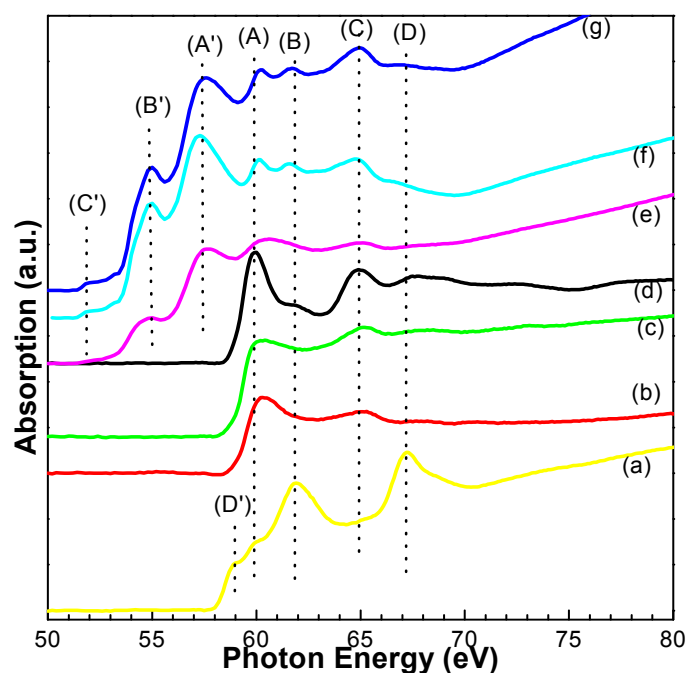


Fig.4 Fluorescence yield (FLY) of Li K edge XANES spectra of the Li containing compounds (a) Li<sub>2</sub>CO<sub>3</sub>, (b) LiPO<sub>3</sub>, (c) Li<sub>4</sub>P<sub>2</sub>O<sub>7</sub>, (d) Li<sub>3</sub>PO<sub>4</sub>, (e) amorphous LiFePO<sub>4</sub>, (f) disordered LiFePO<sub>4</sub>, and (g) crystallite LiFePO<sub>4</sub>, which may appear in the LiFePO<sub>4</sub> based cathode.

It is apparent from Fig.4 that even though, Li<sub>2</sub>CO<sub>3</sub> is one of the precursors often used for the synthesis of LiFePO<sub>4</sub>, due to the change in the atomic environment from carbonate to phosphate, its Li K-edge XANES looks very different from other compounds. The core excitation peak A at around 60.0 eV in spectra of other six phosphates becomes a weak shoulder doublet in the

spectra of  $\text{Li}_2\text{CO}_3$ . Since this peak is related to the unoccupied density of states of Li 2p character, the much reduced intensity of this peak in  $\text{Li}_2\text{CO}_3$  confirms that the localized unoccupied level is partially filled in  $\text{Li}_2\text{CO}_3$ , or the interaction between  $\text{Li}^+$  ion and  $\text{CO}_3^{2-}$  is more covalent; this is in accord with the shift of the threshold to lower energy (the  $\sim 59$  eV shoulder which was not reported previously; it was observed here due to the high resolution of the VLS PGM beamline) as is also in agreement with the results of Tsuji et al.<sup>17</sup> The edge jump is followed by two intense multiple scattering resonance in the spectra of  $\text{Li}_2\text{CO}_3$  62 eV and 67.2 eV. These features arise from multiple scattering of the p wave by the caging environment. More details of the spectroscopic features will be presented elsewhere.

Among the three lithium phosphates,  $\text{Li}_3\text{PO}_4$  exhibits a strong and sharp excitation peak at around 59.9 eV which is consistent with the previous report<sup>17</sup> and has totally four detectable features in the spectra, while both  $\text{Li}_4\text{P}_2\text{O}_7$  and  $\text{LiPO}_3$  show a broadened excitation peak at 60.0 and 60.2, respectively, and show three somewhat broadened main features in the spectra. When the threshold resonance (first peak above the edge, sometimes known as whiteline) in the three lithium phosphates are compared, it can be found that it shifts to higher energy in the order of  $\text{Li}_3\text{PO}_4$  to  $\text{Li}_4\text{P}_2\text{O}_7$  and  $\text{LiPO}_3$ . It has been reported that, the energy position of the Li K-edge depends on the electronegativity of the binding atom in the lithium compound.<sup>39</sup> In our result, it has a linear relationship with the atomic fraction of phosphorus in the material, as shown in Fig. 5, the higher the fraction of phosphorus, the higher is the energy position. Similar trend has been observed in sodium polyphosphate systems.<sup>40</sup>

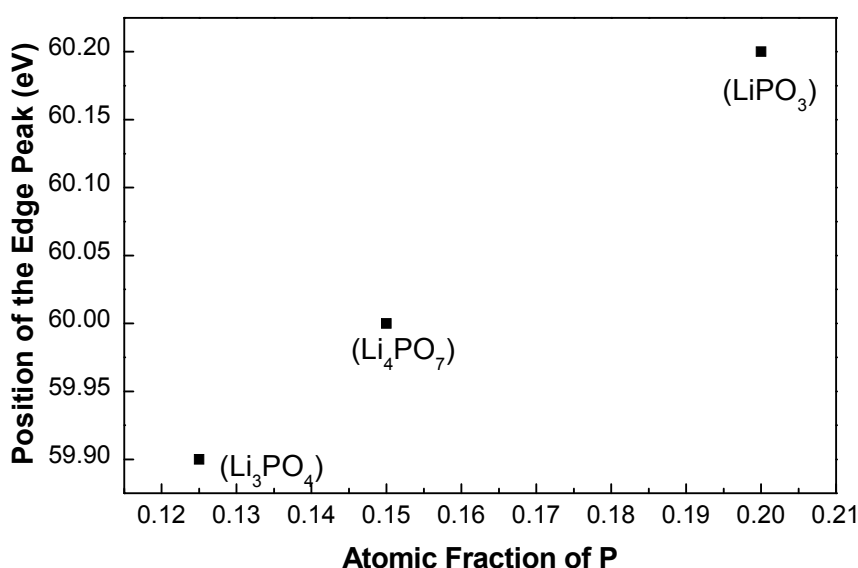


Fig.5 Relationship between the atomic fraction of P in the three lithium phosphates and the position of the edge peak in their Li K-edge XANES

For the  $\text{LiFePO}_4$  (henceforth denoted LFP) materials, except the three peaks, A, B, and C, which also appear in the spectra from  $\text{Li}_3\text{PO}_4$ , a set of three other peaks, marked as A', B' and C' at lower energy are also detected. They are from the Fe  $M_{3,2}$ -edges (3p -3d, 4s transitions). To confirm this, a comparison was made between the XANES of Li K-edge from the c-LFP (crystalline) and the Fe  $M_{2,3}$ -edge from  $\text{Fe}_3(\text{PO}_4)_2$  where both Fe are in the  $\text{Fe}^{2+}$  oxidation state. This is shown in Fig. 6. The Fe  $M_{2,3}$ -edge XANES from  $\text{Fe}_3(\text{PO}_4)_2$  provides convincing evidence that all the three peaks, A', B', and C' are not from Li K-edge, but from the Fe  $M_{2,3}$ -edge. Fortunately, the Li XANES structure can still be revealed by subtracting the  $\text{Fe}_3(\text{PO}_4)_2$  XANES from that of the c-LFP as shown in the difference curve in Fig.6.

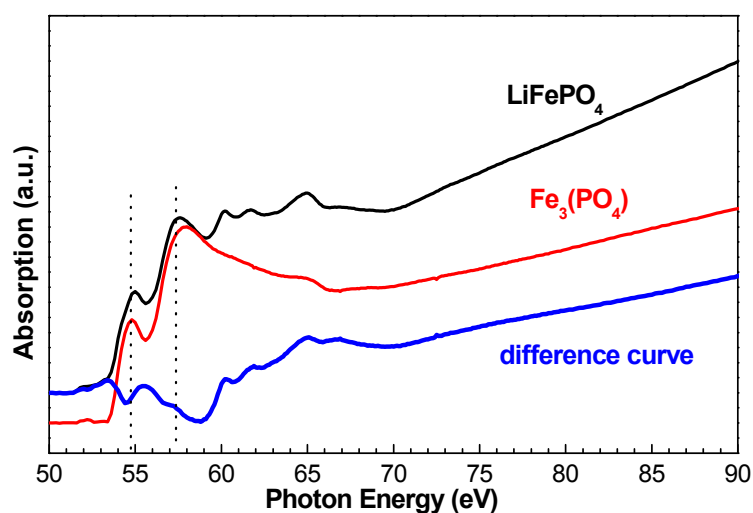


Fig. 6 Comparison of Li K- edge XANES spectra of  $\text{LiFePO}_4$  and  $\text{Fe}_3(\text{PO}_4)_2$ , showing that the peaks at around 52,55 and 57.5 eV in Li K- edge spectra in  $\text{LiFePO}_4$  are resulted from Fe M-edge

From the above results, it can be seen that the Li K-edge XANES spectra of potential lithium phosphate “impurities” as well as  $\text{LiFePO}_4$  are easily discernible. For example, the A and B peak from the c-LFP is much sharper than that of all the three lithium phosphates indicating more

localized states of Li p character. Hence Li *K*-edge XANES is a powerful technique to distinguish between different lithium phosphates from LiFePO<sub>4</sub>. Also among the three LFP samples, the c-LFP (crystalline) and d-LFP (disordered) exhibit spectral patterns much sharper than that of the amorphous, a-LFP; this is expected since the lack of long range order and chemically inhomogeneous local environment of the Li site in the amorphous materials tends to wash out the modulation of the absorption coefficient.

### P *L*-edge XANES

Fig. 7 shows the stacked FLY of P *L*<sub>2,3</sub>-edge XANES spectra of various phosphorus containing reference compounds related to LiFePO<sub>4</sub>, including LiPO<sub>3</sub>, Li<sub>4</sub>P<sub>2</sub>O<sub>7</sub>, Li<sub>3</sub>PO<sub>4</sub>, c-LFP, d-LFP, a-LFP, Fe<sub>3</sub>(PO<sub>4</sub>)<sub>2</sub> and FePO<sub>4</sub>•2H<sub>2</sub>O. The energy positions for peaks of P *L*<sub>2,3</sub>-edge XANES spectra are summarized in a table (see details in Table S1). The TEY data (not shown) are noisy due to charging effects. Compared with the P *K*-edge XANES, which probes the p states, the *L*<sub>3,2</sub>-edge XANES is more informative since it probes the d and s states and has very high energy resolution partly because of the smaller core-hole lifetime broadening, partly because of the high energy resolution photons.<sup>40</sup> The features of a P *L*<sub>2,3</sub>-edge spectrum are generally described by a doublet resonance,<sup>19</sup> labelled as (A) and (B) at the threshold. These two peaks are due to transitions from spin-orbit split 2p electrons (the 2p<sub>3/2</sub> and 2p<sub>1/2</sub> levels), into the first unoccupied 3s like antibonding state.<sup>19</sup> The separation between Peak (A) and peak (B), is the spin orbit coupling. The splitting is an atomic property and usually insensitive to the chemical environment although they have slightly different selection rule (2p<sub>3/2</sub>→3d<sub>5/2,3/2</sub>; 2p<sub>1/2</sub>→3d<sub>3/2</sub>), which becomes important only for high *z* elements with nearly filled d bands. A broad peak (peak (C)) is observed at ~ 2 eV higher photon energy. The assignment of this peak is still controversial although it must be a HOMO +1 state in a molecular description. Ferrett *et al.* assigned this peak to the electron transition to a mixed-valence band.<sup>41</sup> However Harp *et al.* suggested that this peak should be due to transitions to the 3p-like antibonding state as is observed in the Si *L*-edge spectrum of SiO<sub>2</sub>.<sup>42</sup> This assignment is also supported by Hansen *et al.*<sup>43</sup>, and others.<sup>19</sup> Transitions to these dipole forbidden 3p orbitals are possible because they are usually mixed with characters from other elements, such as O and metal. At even higher photon energy a broad and intense peak (peak (F)) owing to 2p to 3d transitions (multiple scattering) can be observed.

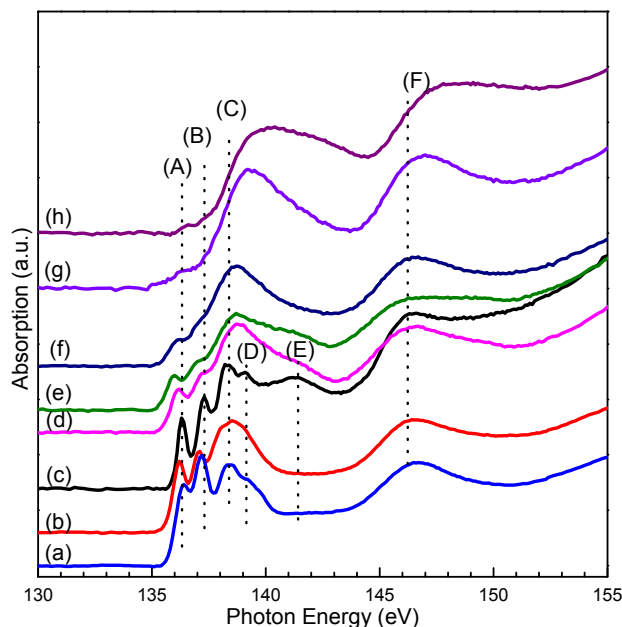


Fig.7 FLY of P  $L_{2,3}$ -edge XANES spectra of the P containing compounds (a)  $\text{LiPO}_3$ , (b)  $\text{Li}_4\text{P}_2\text{O}_7$ , (c)  $\text{Li}_3\text{PO}_4$ , (d) crystallite  $\text{LiFePO}_4$ , (e) disordered  $\text{LiFePO}_4$ , (f) amorphous  $\text{LiFePO}_4$ , (g)  $\text{Fe}_3(\text{PO}_4)_2$  and (h)  $\text{FePO}_4$ , which may appear in the  $\text{LiFePO}_4$  based cathode

Let us return to the spin-orbit doublet resonance at the threshold: peaks (A) and (B) show different profiles for different compounds. In the three lithium phosphates, they are narrow, sharp with high intensity and are clearly visible. A small shift (about 0.1 eV) to the lower energy can be found on these peaks position in the case of  $\text{Li}_4\text{P}_2\text{O}_7$ , compared with  $\text{Li}_3\text{PO}_4$  and  $\text{LiPO}_3$ . Furthermore, the intensity ratio,  $I(\text{B})/I(\text{A})$ , decreases in the order of  $\text{LiPO}_3$ ,  $\text{Li}_3\text{PO}_4$  and  $\text{Li}_4\text{P}_2\text{O}_7$  suggesting different distortion in the crystal field. The change in the intensity of peak (A) and peak (B) in these lithium phosphates arises from the distortion of the phosphate tetrahedral and this behaviour has been successfully used in the analysis of phosphate tribological films.<sup>44</sup> In  $\text{LiFePO}_4$ , these two peaks shift to lower energy relative to the lithium phosphates, and with the obvious decrease in the intensity, they become weak shoulders. Among the three  $\text{LiFePO}_4$  materials, the sharp resonance broadens from c-LFP to d-LFP to a-LFP with a-LFP showing the broadest peaks, characteristic of increasing disorder. In  $\text{Fe}_3(\text{PO}_4)_2$ , with the obvious decrease in

the intensity, peak (A) becomes a weak shoulder and peak (B) is hardly detectable. In  $\text{FePO}_4 \cdot 2\text{H}_2\text{O}$ , these two peaks also present as weak shoulders, and a 0.5 eV shift to a higher energy is observed. This observation indicates that there is more charge redistribution between the phosphate ion and Fe than in lithium phosphate. This result is in agreement with previous results on the P *K*-edge XANES measurement, which showed that during charging with the extraction of  $\text{Li}^+$  from  $\text{LiFePO}_4$ ,<sup>29</sup> the white line of P *K*-edge ( $1s \rightarrow 3p$ ) gradually moved to the high energy side. The major change in  $\text{LiFePO}_4$  during  $\text{Li}^+$  extraction is accompanied by the oxidation of  $\text{Fe}^{2+}$  to  $\text{Fe}^{3+}$ , which results in stronger  $\text{Fe}^{3+}$ -O interaction. In the olivine  $\text{LiFePO}_4$  structure, polarization of the electrons of the oxygen ions towards the phosphorous ions weakens the covalent bonding to the iron ion toward O by the inductive effect. Similarly, the increase in more covalent  $\text{Fe}^{3+}$ -O bonds makes the P-O bonds less covalent by the same inductive effect. The shift of the peaks (A) and (B) doublet to the higher energy side reflects the change in the degree of covalence of the P-O bond altered by the presence of the more covalent  $\text{Fe}^{3+}$ -O bond.<sup>29</sup>

The difference in the Peak (C) is also noticeable among these compounds. In the order of lithium phosphates,  $\text{LiFePO}_4$ , and iron phosphates, the peak shifts to a high energy position and the relative intensity of the peak increases accordingly, while, little difference can be found on the broad peak (F). Except the two iron phosphates, this peak is present at the same energy position for all other materials. This peak is given rise by multiple scattering and a shift to higher energy indicates that in the iron phosphates, especially  $\text{Fe}^{3+}$  phosphates, there is clearly a distortion of the tetrahedron with shorter P-O bond than in the lithium phosphates. It has been shown in simple molecular systems, the energy position of the multiple scattering peaks, or sometimes referred to as shape resonance is inversely to the bond length of the moiety of interest, in this case the P-O inter-atomic distance.<sup>37</sup> In addition, peaks (D) and (E) are prominent in LFP but not noticeable in lithium phosphates. These peaks are clearly associated with the presence of Fe, which is a better electron scatterer than Li. More work need to be done to understand the origin of these two peaks.

It is clear from the above analysis of these spectra, especially peaks (A) and (B) that they can be used to track the presence of various phosphates appeared in the  $\text{LiFePO}_4$  during the synthesis and charge/discharge process.

### **O *K*-edge XANES**

Fig. 8 shows the stacked TEY of the O K-edge XANES of various reference materials relevant to the study of the  $\text{LiFePO}_4$  system. A table (Table S2) is also given to list the detailed position of peaks for the O K-edge. The spectra show a rather broad edge peak with a low intensity pre-edge feature at around 532 eV arising from  $1s \rightarrow \pi^*$  transitions. The major peak at  $\sim 535$  eV has previously been assigned to a transition from the O 1s core level to an unoccupied  $\sigma^*$  orbital of the P-O bond by Nelson *et al.*<sup>45</sup> Since the  $\text{PO}_4^-$  unit exhibits unsaturated P-O bonds and several  $\pi^*$  (bound) and  $\sigma^*$  (quasi bound) are expected.

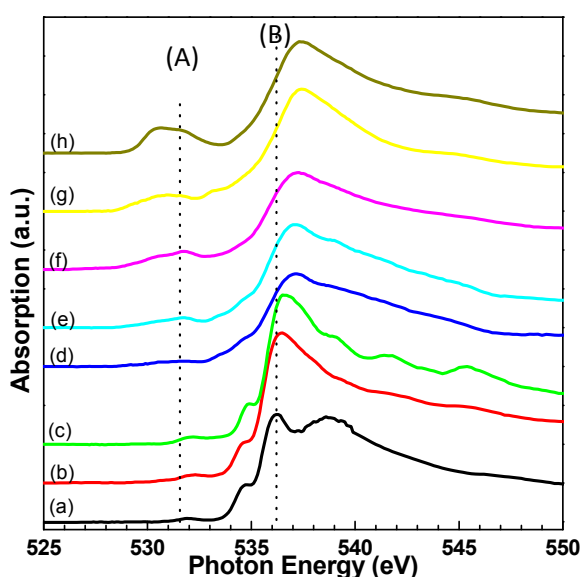


Fig. 8 TEY of O K-edge XANES spectra of the compounds (a)  $\text{LiPO}_3$ , (b)  $\text{Li}_4\text{P}_2\text{O}_7$ , (c)  $\text{Li}_3\text{PO}_4$ , (d) crystallite  $\text{LiFePO}_4$ , (e) disordered  $\text{LiFePO}_4$ , (f) amorphous  $\text{LiFePO}_4$ , (g)  $\text{Fe}_3(\text{PO}_4)_2$ , and (h)  $\text{FePO}_4$

The pre-edge peaks at  $\sim 532$  eV of these spectra correspond to the transition of oxygen 1s electron to the hybridized state of the P 4s, 3p 3d and oxygen 2p orbitals via the resonance structures of  $\text{PO}_3^-$  and  $\text{PO}_4^{3-}$ , thus the unsaturated O-P bond has some  $\pi^*$  character modified by the presence of Fe. In the iron containing phosphates, including  $\text{FePO}_4$ ,  $\text{Fe}_3(\text{PO}_4)_2$ ,  $\text{LiFePO}_4$ , the main peak locates at a higher energy position compared with that of lithium phosphates without iron, including  $\text{LiPO}_3$ ,  $\text{Li}_4\text{P}_2\text{O}_7$  and  $\text{Li}_3\text{PO}_4$ . The reason for the shift is due to the less electropositive iron compared with lithium. Even though, not too much change can be detected

from the main peak of the spectra in these iron containing phosphates, some difference can be found from the pre-edge features, which reflect the degree of un-saturation and polarization of the P-O bond. When there is no lithium in these phosphates, like  $\text{FePO}_4$ ,  $\text{Fe}_3(\text{PO}_4)_2$ , the intensity for the pre-edge peaks increases. Especially,  $\text{FePO}_4$  shows the strongest pre-edge peak among all of these compounds. On the other hand, little difference can be detected from the pre-edge features of the three lithium phosphates, but they can be distinguished from the features at above 535 eV. It is obvious that, at energy above 535 eV, the  $\text{Li}_4\text{P}_2\text{O}_7$  shows the least oscillation, while,  $\text{LiPO}_3$  shows a strong peak at around 537 eV.

### Fe $L_{2,3}$ -edge XANES

The near-edge structure details of the Fe  $L_{2,3}$ -edges for those iron containing compounds, including  $\text{Fe}_2\text{O}_3$ ,  $\text{FePO}_4$ ,  $\text{Fe}_3(\text{PO}_4)_2$  and different  $\text{LiFePO}_4$  are displayed in Fig. 9. Both  $L_3$  and  $L_2$  edges show two main peaks and shoulders (see detail position of peaks marked by dotted lines in Table S3).

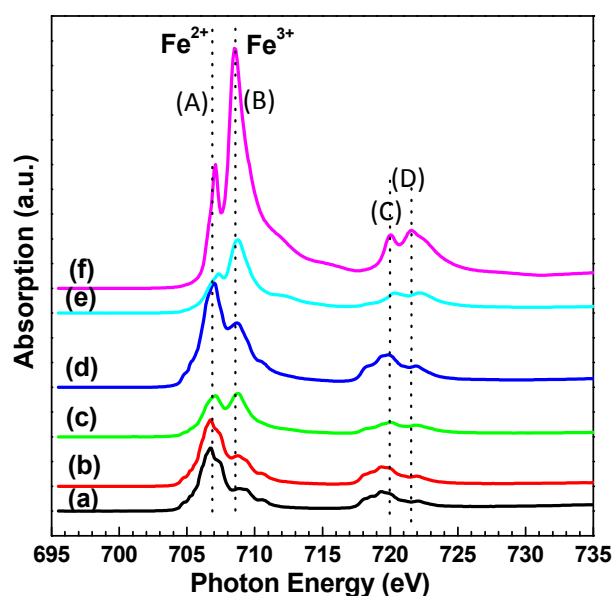


Fig. 9 TEY of Fe  $L_{3,2}$ -edge XANES spectra of the compounds (a) crystallite  $\text{LiFePO}_4$ , (b) disordered  $\text{LiFePO}_4$ , (c) amorphous  $\text{LiFePO}_4$ , (d)  $\text{Fe}_3(\text{PO}_4)_2$ , (e)  $\text{FePO}_4$  and (f)  $\text{Fe}_2\text{O}_3$

Of all the XANES spectra, the Fe  $L_{3,2}$ -edge XANES spectra are perhaps most significant in that it allows us to track the oxidation state of the iron provided all the iron containing

compounds have their characteristic features. The splitting and intensity ratios between the two main peaks come from the interplay of crystal-field, spin-orbit and electronic interactions (Coulomb and exchange)<sup>46</sup>. In fact a multiplet structure is expected although it is convenient to use the most intense peaks for finger print analysis. From Fig. 9, we see that the  $L_3$  edge displays two main peaks at 707.1 eV and 708.5 eV and this pattern is the same for both  $\text{Fe}^{2+}$  and  $\text{Fe}^{3+}$  although the relative intensity is very different. The energy locations are consistent with the results reported in the literature.<sup>47</sup> The spectra from c-LFP and d-LFP are almost the same, showing the main peak at 707.1 eV and a shoulder structure at  $\sim 701.3$  eV. For a-LFP however, the intensities for these two peaks are almost the same, indicating that it may have some  $\text{Fe}^{3+}$  character (see below). The intensity for the second peak of  $\text{Fe}_3(\text{PO}_4)_2$  increases noticeably compared with that from c-LFP and d-LFP. When the oxidation states of iron increased from  $\text{Fe}^{2+}$  to  $\text{Fe}^{3+}$ , in the case of  $\text{FePO}_4$  and  $\text{Fe}_2\text{O}_3$ , the second peak at 708.5 eV becomes the main peak. Again, this analysis clearly shows that different compounds exhibit different but unique spectral features. Thus it is entirely conceivable that we can track all the components, impurity and major components alike.

To further investigate the near surface and bulk region of the specimen, we have employed the IPFY technique as discussed above. It turns out all the IPFY yield exactly the same XANES as those of the TEY except in the case of the amorphous sample, a-LFPO where the IPFY clearly shows more Fe(II) signal compared with the more surface sensitive TEY XANES which shows a significant amount of Fe(III) on the surface. Representative XANES collected from TEY, FLY and IPFY are shown in Fig. 10.

It is apparent from Figure 10 that the FLY is distorted due to self-absorption which is more severe at the Fe  $L_3$  than the  $L_2$  edge while the IPFY for c-LFP and  $\text{Fe}_2\text{O}_3$  are identical to those of TEY except for a small difference in the background. This result suggests that the samples are homogeneous throughout. In the case of a-LFP, the IPFY also exhibits no distortion but an obvious decrease in Fe(III) content indicating that in this particular specimen, the surface is oxidized, while the bulk is still largely Fe(II). Thus, we can reveal the different Fe oxidation state of the surface and the bulk with IPFY if they are indeed different.

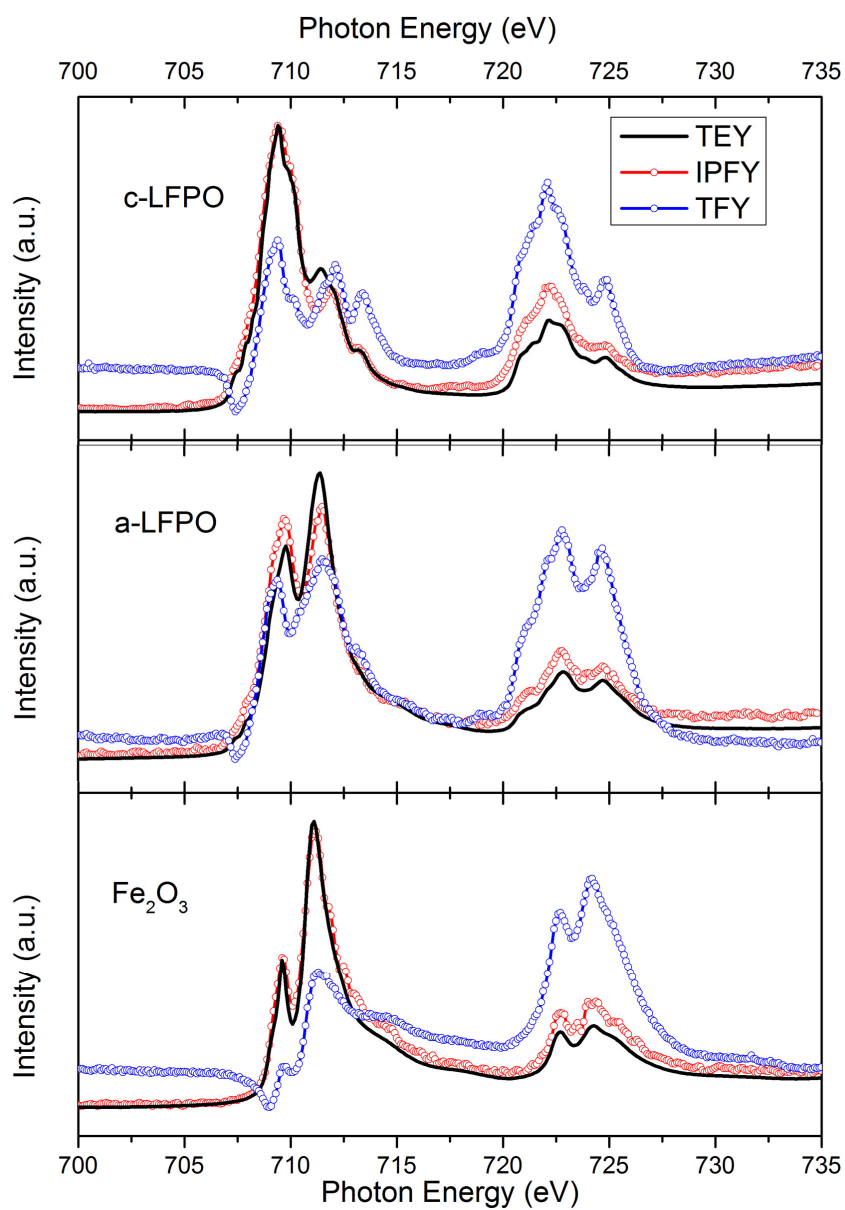


Fig. 10 Comparison of XANES obtained from TEY, FLY and IPFY for c-LFPO, a-LFPO and Fe<sub>2</sub>O<sub>3</sub> showing that IPFY exhibits no distortion from self-absorption which is apparent in

the FLY spectrum and that the a-LFPO is essentially Fe(II) in the bulk although the surface has been oxidized to Fe(III).

## Conclusions

In this work, we have used synchrotron-based soft X-ray absorption spectroscopy to characterize the electronic and chemical structures of various compounds existing in the LiFePO<sub>4</sub> based cathode materials for lithium ion batteries. The XANES of the Li *K*-, O *K*-, P *L*<sub>2,3</sub>- and Fe *L*<sub>2,3</sub>- edges have been recorded and analyzed for all these compounds.

We showed that each element from different compounds displays specific energy positions and spectral features at a given edge accessible by soft x-rays, and hence they can be used as the fingerprint to identify and quantitatively analyze the phase composition during the synthesis and charge/discharge of LiFePO<sub>4</sub>-based cathode materials, which is useful to the understanding of the factors controlling the performance of the batteries and the development of better cathode materials. We also showed that the IPFY technique can be effectively used to characterize the bulk Fe content of the specimen free from self-absorption. The present paper provides an initial glimpse on the unique solution soft X-ray XANES spectroscopy will be able to provide for this problem. More detailed analysis of the experimental data and applications of the technique in studying mixed phases will be reported elsewhere.

## Acknowledgement

This research was supported by Discovery and Engage grants from Natural Sciences and Engineering Research Council of Canada (NSERC), Canada Research Chair (CRC) Program, Canada Foundation for Innovation (CFI), Ontario Innovation Trust (OIT), Ontario Research Fund (ORF), Ontario Early Researcher Award (ERA) and the University of Western Ontario. CLS is supported by CFI, NRC, NSERC, CIHR and the University of Saskatchewan. Technical support from the CLS Staff, Tom Regier, David Chevrier, Lucia Zuin, and Christopher Ryan is gratefully acknowledged.

## Supporting information

Electronic Supplementary Information (ESI) available: Energy position of P L<sub>2,3</sub>-edge, O-K edge and Fe L<sub>2,3</sub>-edge XANES spectra are listed in Tables.

## References

1. A. G. Ritchie, *J. Power Sources* 2001, 96, 1-4.
2. G. Cheruvally, *Lithium Iron Phosphate: A Promising Cathode-Active Materials for Lithium Secondary Batteries*, Trans Tech Publications Ltd., 2008.
3. A. K. Padhi, K. S. Nanjundaswamy and J. B. Goodenough, *J. Electrochem. Soc.*, 1997, 144 (4), 1188-1194.
4. P. P. Prosini, M. LiSi, D. Zane, M. Pasquali, *Solid State Ionics*, 2002, 148 (1), 45-51.
5. T. H. Cho, H. T. Chung, *J. Power Sources*, 2004. 133 (2) 272-276.
6. N. Ravet, J. B. Goodenough, S. Besner, M. Simoneau, P. Hovington, M. Armand, presented at the 196 th Meeting of the Electrochemical Society, Honolulu, HI, October (1999).
7. N. Ravet, Y. Chouinard, J. F. Magnan, S. Besner, M. Gauthier, M. Armand, *J. Power Sources*, 97-98, 503 (2001).
8. J. Wang, X. Sun. *Energy Environ. Sci.* 2012. DOI: 10.1039/C1EE01263K.
9. P. S. Herle, B. Ellis, N. Coombs, and L. F. Nazar, *Nat. Mater.*, 2004, 3, 147-152.
10. S. P. Ong, L. Wang, B. Kang, and G. Ceder, *Chem. Mater.*, 2008, 20, 1798-1807.
11. B. Kang, and G. Ceder, *Nature*, 2009, 458, 190-193.
12. G. Arnold, J. Garche, R. Hemmer, S. Strubele, C. Vogler, M. Wohlfahrt-Mehrens, *J. Power Sources*, 2003, 119-121, 247-251.
13. P. Subramanya Herle, B. Ellis, N. Coombs and L.F. Nazar, *Nature Materials*, 2004, 3, 147-152.
14. Y. Xu, Y. Lu, L. Yan, Z. Yang, R. Yang, *J. Power Sources*, 2006, 160, 570-576.

15. M. S. Song, D. Y. Kim, Y. M. Kang, Y. I. Kim, H. S. Kwon, J. Y. Lee, *J. Power Sources*, 2008, 108 (1) 546-.
16. K. Zaghbi, J. B. Goodenough, A. Mauger, C. Julien, *J. Power Source*, 2009, 194, 1021-1023.
17. J. Tsuji, H. Nakamatsu, T. Mukoyama, K. Kojima, S. Ikeda, and K. Taniguchi, *X-Ray Spectrometry*, 2002, 31, 319-326.
18. C. R. Schulze, and P. M. Bertsch, *Adv. Agron.* 1995, 55, 1-66.
19. J. Kruse, P. Leinweber, K. U. Eckhardt, F. Godlinski, Y. F. Hu, and L. Zuin, *J. Synchrotron Rad.*, 2009, 16 (2) 247-259.
20. R. Dominko, M. Bele, J. M. Coupil, M. Gaberscek, D. Hanzel, I. Arcon, and J. Jamnik, *Chem. Mater.*, 2007, 19 (12), 2960-2969.
21. V. Drozd, G. Q. Liu, R. S. Liu, H. T. Kuo, C. H. Shen, D. S. Shy, X. K. Xing, *J. Alloys Comp.*, 2009, 487 (1-2), 58-63.
22. G. X. Wang, S. Bewlay, S. A. Needham, H. K. Liu, R. S. Liu, V. A. Drozd, J. F. Lee, and J. M. Chen, *J. Electrochem. Soc.*, 2006, 153 (1), A25-A31.
23. A. Deb, U. Bergmann, E. J. Cairns, S. P. Cramer, *J. Phys. Chem. B*, 2004, 108 (22), 7046-7051.
24. A. Deb, U. Bergmann, S. P. Cramer, E. J. Cairns, *Electrochimica Acta*, 2005, 50 (25-26), 5200-5207.
25. A. A. M. Peince, S. Mylswamy, T. S. Chan, R. S. Liu, B. Hannoyer, M. Jean, C. H. Shen, S. M. Huang, J. F. Lee, and G. X. Wang, *Solid State Commun.*, 2004, 132 (7) 455-458.
26. K. F. Hsu, S. K. Hu, C. H. Chen, M. Y. Cheng, S. Y. Tsay, T. C. Chou, H. S. Sheu, J. F. Lee, and B. J. Hwang, *Journal of Power Sources*, 2009, 192 (2), 660-667.
27. A. Hunt, W. Y. Ching, Y. M. Chiang, and A. Moewes, *Phys. Rev. B*, 2006, 73 (20) 205120.
28. M. Giorgetti, M. Berrettoni, S. Scaccia and S. Passerini, *Inorg. Chem*, 2006, 45 (6) 2750-2757.
29. W. S. Yoon, K. Y. Chung, J. McBreen, K. Zaghbi, X. Q. Yang, *Electrochem Solid-State Lett.*, 2004, 9(9), A415-A417. Doi:10.1149/1.2216619.
30. X. J. Wang, H. Y. Chen, X. Q. Yu, L. J. Wu, K. W. Nam, J. M. Bai, H. Li, X. J. Huang, X. Q. Yang. *Chem. Commun.*, 2011, 47, 7170-7172.
31. F. Omenya, N. A. Chernova, S. Upreti, P. Y. Zavalij, K. W. Nam, X. Q. Yang, M. S. Whittingham. *Chem. Mater.*, 2011, 23 (21), 4733-4740.

32. <http://exshare.lightsource.ca/vlspgm/Pages/Specifications.aspx>.
33. <http://exshare.lightsource.ca/sgm/Pages/Beamline.aspx>
34. A. J. Achkar, T. Z. Regier, H. Wadati, Y.-J. Kim, H. Zhang, and D. G. Hawthorn, *Phys Rev. B* 2011, 83 081106(R) .
35. T. K. Sham, *Intl. J. Nanotechnology*, 2008, 5 (9-12), 1194-1246.
36. T.K. Sham and R.A. Holroyd, *Physical Review B*, 1989, 39, 8257.
37. J. Stohr *NEXAFS Spectroscopy*, Springer Verlag Berlin, 1992.
38. Y. M. Yiu and S. L. Yang et al. to be published.
39. J. Tsuji, K. Kojima, S. Ikeda, H. Nakamatsu, T. Mukoyama, and K. Taniguchi, *J. Synchrotron Rad.*, 2001,8, 554.
40. Z. F. Yin, M. Kasarai, and G. M. Bancroft, *Phy. Rev. B*, 1995, 51 (2) 742-750.
41. T. A. Ferrett, M. N. Piancastelli, D. W. Lindle, P. A. Heimann, and D. A. Shirley, *Phys. Rev. A*, 1988, 38 (2) 701-710.
42. G. R. Harp, Z. L. Han, and B. P. Tonner, *J. Vac. Sci. Technol. A*, 1990, 8 (3) 2566-2569.
43. P. L. Hansen, R. Brydson, and D. W. McComb, *Microsc. Microanal. Microstruct.*,1992, 3, 213-219.
44. M. Kasarai, Z. Yin, G. M. Bancroft, K. Fyfe and K. H. Tan, *J. Phys IV France*, 1997, 7, C2-847-849.
45. A. J. Nelson, T. van Buuren, E. Miller, T. A. Land, C. Bostedt, N. Franco, P. K. Whitman, P. A. Baisden, L. J. Terminello, T. A. Callcott, *J. Electron Spectrosc. Relat. Phenom.*, 2001,114-116, 873-116.
46. G. van der Laan and I. W. Kirkman, *J. Phys. Condens. Matter.*, 1992, 4 (16) 4189-4204.
47. R. K. Hocking, E. C. Wasinger, F. M. F. de Groot, K. O. Hodgson, B. Hedman, and E. I. Solomon, *J. Am. Chem. Soc.*, 2006, 128 (32) 10442-10451.